NUMERICAL MODELING OF MACROSEGREGATION DURING THE DIRECT-CHILL CASTING OF AN AL ALLOY BILLET

A. Jafari[1,2], S. H. Seyedein[1], M. R. Aboutalebi[1,*], D. G. Eskin[2] and L. Katgerman[2]
* mrezab@iust.ac.ir
Received: April 2010 **Accepted: August 2010**

1 Centre of Excellence for Advanced Materials and processing, School of Metallurgy and Materials Engineering, Iran University of Science and Technology, Tehran, Iran.
2 Dept. of Materials Science and Engineering, Delft University of Technology (TUDelft), 2628 CD Delft, The Netherlands.

Abstract: *Macrosegregation has been received high attention in the solidification modeling studies. In the present work, a numerical model was developed to predict the macrosegregation during the DC Casting of an Al-4.5wt%Cu billet. The mathematical model developed in this study consists of mass, momentum, energy and species conservation equations for a two-phase mixture of liquid and solid in axisymmetric coordinates. The solution methodology is based on a standard Finite Volume Method. A new scheme called Semi-Implicit Method for Thermodynamically-Linked Equations (SIMTLE) was employed to link energy and species equations with phase diagram of the alloying system. The model was tested by experimental data extracted from an industrial scale DC caster and a relatively good agreement was obtained. It was concluded that a proper macrosegregation model needs two key features: a precise flow description in the two-phase regions and a capable efficient numerical scheme.*

Keywords: *Macrosegregation, Modeling, Solidification, DC Casting, Aluminum Alloys.*

1. INTRODUCTION

Wrought ingots of Aluminum alloys are widely produced via semi-continuous Direct-Chill casting process which has been identified as the most commercially efficient technology for large-size ingots [1]. An important issue associated with this process has always been macrosegregation, from which problems in quality and limitations in productivity arise. Comprehensive reviews on macrosegregation are available in the literature [2,3]. Macrosegregation is defined as a non-uniform chemical composition along the practical scales (>1 cm) of the cast product. In spite of the microsegregation, which is appeared in the scales of the microstructure (<1 mm) and can be eliminated by a heat treatment (i.e. homogenization process), macrosegregation will remain within the product as an irreversible defect. Thus, the control of macrosegregation during DC casting process has been received high attention by researchers [1] in a wide range of experimental and numerical quest. Devadas and Grandfield [4] used a Finite Elements Model to study the DC casting of aluminum alloys. Du et al [5] implemented a multi-component macrosegregation modeling to a DC casting of an Al-Cu-Mg alloy. They indicated that the contribution of each of solute elements to the solutal buoyancy affects the final macrosegregation pattern. Among the general experimental and numerical data available for macrosegregation in DC casting, an analysis was performed by Eskin et al [6]. They found a scaling relationship between the magnitude and direction of centerline segregation in cast billets and the process parameters, i.e., billet diameter and casting speed. It seems that there is a range of these process parameters where the centerline segregation is positive, and there is a threshold when the centerline segregation vanishes. Reddy [7] investigated the macrosegregation in DC casting with a two-phase simulation, considering solid grain transport, solutal undercooling, microsegregation and grain impingement. A simple instantaneous nucleation model was used in his work. The results indicated that, grain transport promoted the negative centerline segregation while the shrinkage flow led to inverse segregation. A more permeable mushy zone was shown to positively segregate copper in the ingot centre region. Concentrating the exudation of enriched droplets on the surface of ingot during DC casting, Mo [8] established a

one dimensional mathematical mode1 for the development of exudated droplets. In his model, metallostatic pressure driven interdendritic melt flow through the mushy zone was considered by a Darcy type equation. The decrease of the total solute concentration is also considered, as a consequence of the positive surface segregation. Nadella et al [1] have recently reviewed the mechanisms of macrosegregation and their correlation with DC casting process parameters and structural features. The role of grain refining in macrosegregation has also been studied by Nadella et al [9]. In an effort to develop a comprehensive numerical model for the casting of alloys, Rerko et al [10] established an experimental solidification study to generate controlled benchmark data as well as to observe the phenomena. They examined transport of the equiaxed grains, effects of solid transport and thermosolutal convection on macrosegregation and grain size distribution patterns. Krane and Vusanovic [11] applied a macrosegregation model to a horizontal direct chill casting (HDC) of an Aluminum-Copper alloy, where buoyancy acted perpendicularly to the casting direction and significant asymmetry was seen in the flow patterns and macrosegregation profiles. Focusing on numerical complexities of the problem, Venneker and Katgerman [12] addressed numerical diffusion in the computed results of the macrosegregation models and gave a comparison between the results of various numerical differencing schemes, regarding the minimum error. Vreeman and Incropera [13] explained a consistent discretization procedure in the numerical modeling of macrosegregation and performed a sample calculation on DC casting of an Al-Cu billet. Vreeman et al [14] investigated the macrosegregation in an industrial scale Al-6%Cu billet by modeling and experiments. They considered the transport of free-floating dendrites in their model to investigate the effects of grain refining on the macrosegregation. Zaloznik and Sarler [15] have implemented more accurate differencing scheme (ULTRA-QUICK) for the solution of the velocity field, in contrast to popular but inaccurate first-order upwind discretization methods, widely used. They obtained a more intricate flow structure and additional circulation cells than that of previously known in the bottom of the liquid pool of DC casting machine [16]. A mixture model was proposed by Vreeman et al [17, 18] to account for the redistribution of alloying elements through the transport of free-floating dendrites as well as flow in the mushy zones of a solidifying ingot. They indicated that the flow of liquid and free-floating dendrites were controlled by a balance between buoyancy forces arising from mixture density variations and the development of an adverse pressure gradient.

So far, immense attempts on the subject, although it is not enough yet, have brought a good insight of the problem to the researchers. With a general look into applied numerical models, it can be seen that simple widely-used methods are not able to handle physical complexities. On the other hand, realistic and detailed numerical methodologies are specified to the very similar presented cases, which are numerous and not efficient in general practice. What is thought to be a need among various models is a well-established capable solution methodology for the wide range of complexity of mathematical description of the problem. The present work has been then undertaken to solve the problem again, in a manner which is giving a simple general methodology toward the complex nature of the problem, but keeping the model efficient in implementation.

The problem deals with the heat transfer, fluid flow, solute transport and solidification of binary alloy Al-Cu melt introduced into a model of industrial DC caster producing 195 mm-diameter round billets. Liquid metal is fed to the caster from top and cooled from sides in two parts (i.e. primary cooling in the mold and secondary cooling in direct contact with water). Then it is solidified and leaves the caster from the bottom. Within the solidifying billet, different phenomena are taking place that make the fluid flow complex. As liquid metal is cooled under the liquidus temperature thermodynamically, solid dendrites form and float in the melt. The dendrites then branch and grow by thermal and solutal cooling. In the current problem, it is assumed that the dendrites move with the same velocity as the melt. The liquid-solid mixture is

seen as a pseudo-liquid two-phase fluid, i.e. slurry. Due to different density of the phases and at different temperature and compositions, thermosolutal convection is generated in the slurry. As soon as the growing dendrites meet each other at the tip of the branches, they attach together and become coherent, forming a big porous rigid structure called mush. Thereafter, the two-phase mixture is considered to be a fluid flowing through a porous structure which is moving at the casting speed. In the mushy zone, a shrinkage-driven flow moves the melt through the solid network due to the different density of the phases.

2. MATHEMATICAL MODELING

Assumptions. The following assumptions were considered to mathematically describe the problem; (a) Because of the symmetry in θ direction, 2-D axisymmetric coordinates were assumed to represent the process. (b) The fluid flow is laminar regarding the inlet dimensions and velocity. (c) All phenomena and quantities within the domain are assumed to be independent of time, i.e. the problem is at steady-state. (d) The material is considered as a two-phase mixture of liquid-solid Aluminum alloy. The liquid metal is then assumed to behave as a Newtonian fluid. (e) No-slip conditions were assumed at solid boundaries. (f) The solid dendrites were taken as a pseudo-fluid in the slurry free-floating zone, where they move at the same velocity as the liquid moves. (g) The materials properties, specifically the density, are different for liquid and solid. The densities also vary with temperature, which is considered with coefficients of thermal expansion for the liquid and the solid. Figure 1 shows the computational domain of the problem.

Governing equations. Regarding the presence of a liquid/solid mixture material in the process, a volume fraction, ε_j, and a mass fraction, fj, is defined for each phase, while $\varepsilon_L+\varepsilon_S=1$ and $f_L+f_S=1$. The mathematical modeling of the problem consists of the following conservation equations for mixture variables [19]:

Continuity:

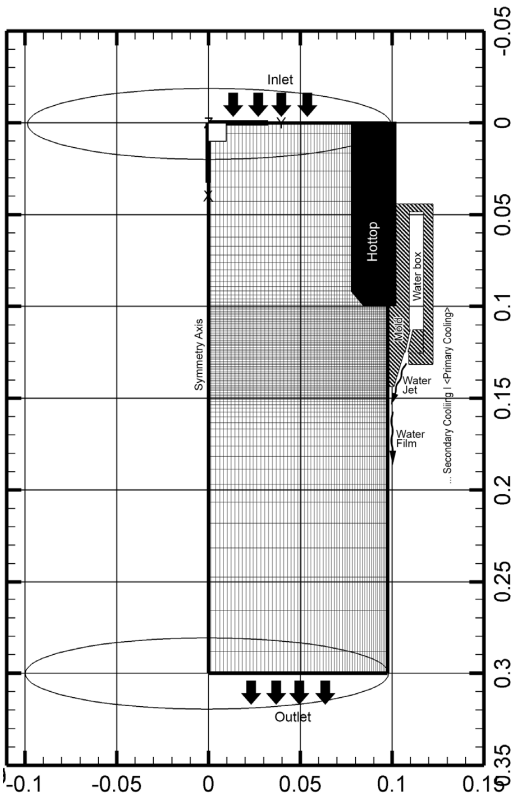

Fig. 1. Computational domain of the problem.

$$\frac{\partial}{\partial z}(\rho u)+\frac{1}{r}\frac{\partial}{\partial r}(r\rho v)=0 \tag{1}$$

Momentum z:

$$\frac{\partial}{\partial z}(\rho uu)+\frac{1}{r}\frac{\partial}{\partial r}(r\rho vu)= \frac{\partial}{\partial z}\left(\mu'\frac{\partial u}{\partial z}\right)+\frac{1}{r}\frac{\partial}{\partial r}\left(r\mu'\frac{\partial u}{\partial r}\right)-\frac{\partial P}{\partial z} +B+M_z \tag{2}$$

Momentum r:

$$\frac{\partial}{\partial z}(\rho uv)+\frac{1}{r}\frac{\partial}{\partial r}(r\rho vv)= \frac{\partial}{\partial z}\left(\mu'\frac{\partial v}{\partial z}\right)+\frac{1}{r}\frac{\partial}{\partial r}\left(r\mu'\frac{\partial v}{\partial r}\right)-\frac{\partial P}{\partial r} -\mu'\frac{v}{r^2}+M_r \tag{3}$$

Energy:

$$\frac{\partial}{\partial z}(\rho u h)+\frac{1}{r}\frac{\partial}{\partial r}(r\rho v h)= \\ \frac{\partial}{\partial z}\left(\frac{k}{c}\frac{\partial h}{\partial z}\right)+\frac{1}{r}\frac{\partial}{\partial r}\left(r\frac{k}{c}\frac{\partial w}{\partial r}\right)+F^{h}+D^{h} \tag{4}$$

Species:

$$\frac{\partial}{\partial z}(\rho u C)+\frac{1}{r}\frac{\partial}{\partial r}(r\rho v C)= \\ \frac{\partial}{\partial z}\left(\rho D\frac{\partial C}{\partial z}\right)+\frac{1}{r}\frac{\partial}{\partial r}\left(r\rho D\frac{\partial C}{\partial r}\right)+F^{C}+D^{C} \tag{5}$$

In Equation (3) and (4), energy and species source terms D^{ϕ} and F^{ϕ} are diffusion-like and convection-like mixture sources [13] derived as:

$$D^{h}=-\nabla\cdot\left(\frac{k}{c}\nabla h\right)+\nabla\cdot(k\nabla T) \\ F^{h}=\nabla\cdot(\rho\mathbf{v}h)-\sum_{j=\mathrm{L,S}}\nabla\cdot\left(\varepsilon_j\rho_j\mathbf{v}_j h_j\right) \\ D^{C}=-\nabla\cdot(\rho D\nabla C)+\sum_{j=\mathrm{L,S}}\nabla\cdot\left(f_j\rho_j D_j\nabla C_j\right) \\ F^{C}=\nabla\cdot(\rho\mathbf{v}C)-\sum_{j=\mathrm{L,S}}\nabla\cdot\left(\varepsilon_j\rho_j\mathbf{v}_j C_j\right) \tag{6}$$

The solid volume fraction, ε_{S}, is calculated from its counterpart mass fraction as:

$$\varepsilon_{\mathrm{S}}=f_{\mathrm{S}}\rho/\rho_{\mathrm{S}} \tag{7}$$

The solid mass fraction, f_{S}, is calculated via the thermodynamics of the phase change which is introduced later in the text. The mixture dependent variables in the conservation equations are considered as:

$$\mathbf{v}=f_{\mathrm{L}}\mathbf{v}_{\mathrm{L}}+f_{\mathrm{S}}\mathbf{v}_{\mathrm{S}} \\ h=f_{\mathrm{L}}h_{\mathrm{L}}+f_{\mathrm{S}}h_{\mathrm{S}} \\ C=f_{\mathrm{L}}C_{\mathrm{L}}+f_{\mathrm{S}}C_{\mathrm{S}} \tag{8}$$

And mixture material properties are defined as:

$$\rho=\varepsilon_{\mathrm{L}}\rho_{\mathrm{L}}+\varepsilon_{\mathrm{S}}\rho_{\mathrm{S}} \qquad ,c=f_{\mathrm{L}}c_{\mathrm{L}}+f_{\mathrm{S}}c_{\mathrm{S}} \\ k=\varepsilon_{\mathrm{L}}k_{\mathrm{L}}+\varepsilon_{\mathrm{S}}k_{\mathrm{S}} \qquad ,D=f_{\mathrm{L}}D_{\mathrm{L}}+f_{\mathrm{S}}D_{\mathrm{S}} \tag{9}$$

A packing solid fraction, $\varepsilon_{\mathrm{SP}}$, is defined above which the solid dendrites attach together and becomes a rigid network ($\mu_{\mathrm{S}}\to\infty$). Thereafter, liquid flows through this porous structure due to the shrinkage force. The viscose property of the mixture is modeled as Ni et al [20, 21]:

$$\mu'=\frac{\rho}{\rho_{\mathrm{L}}}\mu \\ \mu=\begin{cases}\mu_{\mathrm{L}}\left(1-\dfrac{\varepsilon_{\mathrm{S}}}{\varepsilon_{\mathrm{SP}}}\right)^{-2.5\varepsilon_{\mathrm{SP}}} & ,\varepsilon_{\mathrm{S}}<\varepsilon_{\mathrm{SP}}\\ \mu_{\mathrm{L}} & ,\varepsilon_{\mathrm{S}}\geq\varepsilon_{\mathrm{SP}}\end{cases} \tag{10}$$

Momentum source terms B in Equation (2) stand for gravity force in the slurry zone ($\varepsilon_{\mathrm{S}}<\varepsilon_{\mathrm{SP}}$) in terms of thermosolutal buoyancies as [18]:

$$\mathbf{B}=\varepsilon_{\mathrm{L}}\rho_{\mathrm{L}}\mathbf{g}\left[\beta_{\mathrm{L}}^{\mathrm{T}}(T-T_{\mathrm{ref}})+\beta_{\mathrm{L}}^{C}(C_{\mathrm{L}}-C_{\mathrm{ref}})\right] \\ +\varepsilon_{\mathrm{S}}\rho_{\mathrm{S}}\mathbf{g}\left[\beta_{\mathrm{S}}^{\mathrm{T}}(T-T_{\mathrm{ref}})+\beta_{\mathrm{S}}^{C}(C_{\mathrm{S}}-C_{\mathrm{ref}})\right] \\ +\varepsilon_{\mathrm{S}}(\rho_{\mathrm{S}}-\rho_{\mathrm{L}})\mathbf{g} \\ \varepsilon_{\mathrm{S}}<\varepsilon_{\mathrm{SP}} \tag{11}$$

In the case of rigid porous mushy zone (i.e. $\varepsilon_{\mathrm{S}}\geq\varepsilon_{\mathrm{SP}}$), the last two terms of Equation (11) will be omitted. Momentum source terms M in Equation (2) and (3) stand for interfacial drag force in mushy zone ($\varepsilon_{\mathrm{S}}\geq\varepsilon_{\mathrm{SP}}$) which is defined as a damping Darcy source in porous mushy structure [22]:

$$\mathbf{M}=-\frac{\rho}{\rho_{\mathrm{L}}}\frac{\mu}{K}(\mathbf{v}-\mathbf{v}_{\mathrm{S}}) \tag{12}$$

Where K is the permeability of the porous structure, defined from Kozeny-Carman expression [23] as:

$$K=\frac{1}{5S_{\mathrm{i}}^{\mathrm{V}}}\frac{(1-\varepsilon_{\mathrm{S}})^{3}}{\varepsilon_{\mathrm{S}}^{2}} \tag{13}$$

The interfacial area concentration, $S_{\mathrm{i}}^{\mathrm{V}}$, depends on the geometry and density of the solid dendrites at each position. Using $S_{\mathrm{i}}^{\mathrm{V}}$ in permeability term K, the effect of microstructure on the flow pattern can be implicitly modeled. Assuming a constant grain density and equiaxed dendritic grains, $S_{\mathrm{i}}^{\mathrm{V}}$ can be modeled as [24]:

$$S_{\mathrm{i}}^{\mathrm{V}}=G^{a}\varepsilon_{\mathrm{S}}{}^{b}F^{c} \\ G=36\pi n \qquad ,F=\frac{1-\max[\varepsilon_{\mathrm{S}},\varepsilon_{\mathrm{SP}}]}{1-\varepsilon_{\mathrm{SP}}} \\ a=\tfrac{1}{3} \quad ,b=\tfrac{2}{3} \quad ,c=\tfrac{2}{3} \tag{14}$$

Table 1. Cooling parameters for DC casting process [25]

Cooling region	**Position** (mm)	$H_{Cooling}$ (W/m^{2}K)	$T_{Cooling}$ (K)
Hot-top	$0 < z < 100$	0	-
Mold (Primary cooling)	$100 < z < 145$		
Liquid Contact	$\varepsilon_S \leq 1$	5000	318
Air Gap	$\varepsilon_S > 1$	2500	523
Water (Secondary cooling)	$145 < z < 300$		
Air Gap	$145 < z < 150$	3000	318
Jet Impingement	$150 < z < 159$	10,000	318
Water film	$z > 159$	10,000	318

Where n is the grain density. For a grain size of d = 200 μm in the observed solid structure, the number of spherical grains per 1 cubic meter can be calculated as:

$$n = \frac{0.74}{36\pi d^3} \tag{15}$$

Equation (13) gives an interface area concentration regarding the growth of dendrites before the coherency and the coarsening of dendrites after the coherency.

According to the thermodynamics, the mixture enthalpy, h, is defined to be the extensive heat content which is the summation of latent heat (or mixture reference enthalpy, h^{ref}) and sensible heat:

$$h = h^{ref} + cT \tag{16}$$

Since h is obtained from the energy equation (3), Equation (15) is used to calculate temperature as:

$$T = \frac{h - h^{ref}}{c} \tag{17}$$

Where h^{ref} is calculated from the mixture rule as:

$$h^{ref} = f_L h_L^{ref} + f_S h_S^{ref} \tag{18}$$

Other necessary relations in the thermodynamics of the phase change problem are the phase diagram relations. In the past literature, phase diagrams has been involved in solidification models in terms of the concept of partition coefficient and intermediate relations for solidification like linear lever-rule and eutectic expressions. In this work, however, the phase diagram is involved simply in the original form of equilibrium lines as:

$$T = -1990.076C + 933.5 \quad \text{S-L: Solidus Curve} \tag{19}$$

$$T = -308.5598C^2 - 238.4783C + 933.5 \quad \text{L-S: Liquidus Curve} \tag{20}$$

Where C is considered as the mass fraction of the species (e.g. 0.05 for 5wt%Cu) and T is obtained in K.

Boundary Conditions. Boundaries of the problem are inlet, outlet, cooling side and symmetry axis as shown in ?Figure 1. At the outlet, the casting velocity is applied. The domain is long enough that the cooling effects of outlet on the process can be ignored. Thus, the outlet is assumed to be thermally adiabatic. A zero composition gradient is also reasonable for the species equation at the outlet, where no change happens in the macroscopic composition of the billet. At the inlet, a constant uniform velocity is applied so that the overall mass is balanced regarding the known outlet. There, the temperature and the composition are set for the inlet molten Aluminum alloy. For the symmetry axis, zero gradients for temperature, composition and tangential velocity are assumed. The perpendicular velocity is set to zero across the symmetry axis. At the cooling side, no-slip conditions are assumed on the internal wall of hot-top and mold. However, all solid velocities after the coherency of dendrites are supposed to be identical to the casting velocity. The heat transfer across the cooling side of the domain is generally modeled via a heat transfer coefficient and convection on the surface as:

$$q_{\text{Cooling}} = -H_{\text{Cooling}}\left(T_{\text{Cooling}} - T\right) \tag{21}$$

The heat transfer coefficient, H, and the ambient temperature, T_∞, vary over the different regions of the cooling side. ?Table 1 lists the cooling parameters applied on this boundary. The hot top is made of a refractory material through which the heat transfer is ignored. As can be seen in Figure 1, a part of the hot-top is located within the domain at the cooling side. This part is blocked against heat and fluid flow and the internal boundaries are kept adiabatic.

3. SOLUTION METHODOLOGY

A Control-Volume based Finite Difference Method (CV-FDM) was used to discretize differential equations [26, 27]. A FORTRAN code was developed to perform the calculations and solve the discretized equations. A non-uniform fixed grid is employed (as shown in ?Figure 1) and has been found to give an efficient accuracy in the order of 140×80 nodes refined at higher radii and in two-phase regions. The conservation equations (1) to (4) were written for a control volume and were put in the general form of [27]:

$$\frac{\partial(\rho\phi)}{\partial t} + \nabla\cdot(\rho\mathbf{v}\phi) = \nabla\cdot(\Gamma_\phi\nabla\phi) + S^\phi \tag{22}$$

Where ϕ is a general dependent variable, and Γ_ϕ and S^ϕ are defined as relevant diffusion coefficient and source terms regarding the specific conservation equation. Then, the equations were discretized over a typical axisymmetric control volume to obtain a set of algebraic equations for each equation. Applying an under-relaxation, the general form of discretized equation obtained as:

$$\begin{aligned}
&a_{\text{P}}\phi_{\text{P}} = \sum a_{\text{nb}}\phi_{\text{NB}} + b \quad \text{, NB=E,W,N,S}\\
&a_{\text{nb}} = D_{\text{nb}} + \max\left[-F_{\text{nb}}, 0\right]\\
&a_{\text{P}} = \left(\sum a_{\text{nb}} - S_{\text{P}}\Delta V\right)/\alpha\\
&b = S_{\text{C}}\Delta V + (1-\alpha)a_{\text{p}}\phi_{\text{P}}\\
&D_{\text{nb}} = \left(\frac{\Gamma A}{\delta}\right)_{\text{nb}},\ F_{\text{nb}} = (\rho\mathbf{v}A)_{\text{nb}}
\end{aligned} \tag{23}$$

Some of the volumes are located in the hot-top region within the domain. Those volumes were treated as obstacles to heat and fluid flow, using block-off technique. UPWIND scheme was adopted to calculate convective values between nodes. To link the velocity and pressure field, SIMPLEC method by Patankar [27] was employed in the code. So far the case was treated as a standard CFD problem. One issue, that makes the macrosegregation problems special, is the calculation of solid fraction which is derived from a link between energy and species equations and thermodynamics of the phases. For calculation of the solid fraction a recent thermodynamic updating scheme was used, called Semi-Implicit Method for Thermodynamically-Linked Equations (SIMTLE) [28]. With this method, the phase diagram data are involved by the original form of equilibrium curves as Equations (18) and (19). Eutectic solidification is considered as well as primary solidification through a five-step simple technique in SIMTLE:

1. Calculation of temperature.

$$T = \left(h - h^{\text{ref}}\right)/c \tag{24}$$

2. Calculation of the composition of solid on the phase diagram:

$$C_{\text{S}} = \mathbf{f}^{C}_{\text{Solidus}}(T) \quad \text{from Equation (18)} \tag{25}$$

3. Calculation of the composition of liquid (the primary phase):

$$C_{\text{L}} = \left(C - f_{\text{S}}C_{\text{S}}\right)/f_{\text{L}} \tag{26}$$

4. Calculation of the Dynamic Implicit Equilibrium Temperature (DIET):

$$T^{\text{eq}} = \mathbf{f}^{T}_{\text{Liquidus}}(C_{\text{L}}) \ \text{from Equation (19)} \tag{27}$$

5. Calculation of the correction for solid mass fraction:

$$f'_{\text{S}} = \frac{c\left(T - T^{\text{eq}}\right)}{\Delta h^{\text{ref}}_{\text{L}\to\text{S}} + T^{\text{eq}}\Delta c_{\text{L}\to\text{S}}} \quad ,\Delta c_{\text{L}\to\text{S}} =$$

$$c_S - c_L, \Delta h_{L\to S}^{ref} = h_S^{ref} - h_L^{ref} \quad (28)$$

When the correction is obtained, it is applied to the current solid fraction as:

$$f_S^{new} = f_S + \lambda f_S' \quad (29)$$

Where λ is a relaxation factor, found to be λ=1-f_S to get a stable convergence [28]. The updating scheme, Equations (23) to (28), is repeated two times at each iteration of macroscopic solutions. This number was chosen to achieve an efficient solution. A high number of repeats, during the solution, forces the quantities toward a strict thermodynamic equilibrium, which impose an excessive internal iteration. This gives no interest, while the quantities are far from the desired solution. However, the final solution will be independent of the number of the iteration when the quantities reach a stable amount.

Finally, the algebraic equations were solved using line by line TDMA method. The convergence criterion considered for the residuals of the equations was as follow:

$$R = \left[\sum_{v,p,h,C} \left(\sum_{P} | a_P \phi_P - \sum_{nb} a_{nb} \phi_{nb} - b | \right) + \sum_{P} | f_S' | \right] < 10^{-2} \quad (30)$$

Using the Gauss' integral, in addition of the convergence criteria, the overall misbalance between the input and output of energy was found to be less than ~1000 J/m^{3}s and that of species was found to be less than 10^{-3} Kg/m^{3}s as the calculation meets the convergence criteria. The material properties and process parameters, used in the model are listed in Table 2.

4. RESULTS AND DISCUSSION

The model was adjusted and successfully executed for an industrial scale DC casting. To assure the performance of the heat flow and solidification model firstly, the solidification profile was studied for a case in which a Al-3.7%Cu billet is formed at a casting speed of 7

Table 2. Material properties of Aluminum alloy used in the model.

Material Properties	**Values**	
Liquid density, ρ_L	2460 kg/m^3	
Solid density, ρ_S	2750 kg/m^3	
Liquid specific heat, c_L	1054 J/kgK	
Solid specific heat, c_S	958 J/kgK	
Liquid thermal Conductivity, k_L	95 W/mK	
Solid thermal Conductivity, k_S	180 W/mK	
Latent heat of fusion, $h_L^{ref} - h_S^{ref}$	390 kJ/kg	
Liquid diffusion coefficient, D_L	5×10^{-9} m^2/s	
Solid diffusion coefficient, D_S	0 m^2/s	
Liquid viscosity, μ_L	0.0013 kg/ms	
Thermal expansion coefficient, β_T	-1.17×10^{-4} K^{-1}	
Solutal expansion coefficient, β_C	0.73	
Eutectic composition, C_e	33.0 wt%	
Phase diagram relations,		
$\mathbf{f}^T_{Liquidus}$	Equation (19)	
$\mathbf{f}^T_{Solidus}$	Equation (18)	
$\mathbf{f}^C_{Liquidus}$	$\mathbf{f}^T_{Liquidus}{}^{-1}$	
$\mathbf{f}^C_{Solidus}$	$\mathbf{f}^T_{Solidus}{}^{-1}$	
Process Parameters	**Case I**	**Case II**
Casting velocity, u_C	7 cm/min	12 cm/min
Inlet temperature , T_0	985 K	985 K
Inlet composition, C_0	3.7 wt%	3.7 wt%

cm/min (Case I in Table 2). The case was chosen according to previous experimental investigation of the solidification profile performed on the DC casting machine. To capture the solidification front during the casting, an amount of grain refiner was suddenly added to the molten metal pool in the mold. The grain refiner immediately changes the solidifying grain structure within the slurry region. This change can then be observed as a solidification front in the macro-etched longitudinal section of the billet. It can be said that the observed profile indicates the coherency line at the moment of grain refining practice. The model was run based on Case I and the predicted solidification profile was compared with the experiments, which is shown in Figure 2. Flow pattern and solid fraction contours are readily shown in Figure 2. The contour ε_S=0.3 indicates the computed position of coherency surface, where the superimposed data points shows the experimentally observed positions of the coherency obtained by the grain refining practice. The numerical position of the coherency line shows adequate agreement with the experimental data to rely the model in capturing different flow regions in the domain. It should also be stressed that the exact position where the dendrites become coherent is very hard to detect because of complex phenomena of dendrite impingements and fragmentations. Though, the solidification front experimentally detected, gives a good estimation of transition between the flow regions of slurry and mushy.

Figure 3 shows the computed results for the casting conditions of case II of which the parameters are closer to an industrial DC casting. Again, the contour ε_S = 0.3 shows the coherency contour or solidification front. In Figure 3a the computed flow pattern is illustrated where a key feature of the Al DC casting process can be seen, that is the thermosolutal recirculation about the periphery. The molten aluminum moves in this vortex, being driven by heavy enriched and cooled metal, with a speed more than five times the casting velocity. In the central parts, however, there is not that much thermal and solutal gradient. Therefore, the flow is governed by the effect of free-floating dendrites and inertia at the central slurry region. The movement of free-floating dendrites is not considered within current model, which should be mentioned for the obtained flow pattern.

Figure 3b shows the temperature distribution in the solidifying billet. A sharp thermal gradient can be seen within the narrow mushy zone, while a more thermally uniform slurry zone is clear. This has been characterized before by Nadella et al as the specifications of slurry and mushy regions [1]. Another feature in ?Figure 3b is a macroscopic thermal layer just above the slurry region in the form of an axial temperature gradient which separates the molten aluminum in the hottop and in the solidification region [29]. The consequent flow within this macroscopic thermal layer is shown in Figure 3a which is radial toward the mold wall. This flow leads the fresh melt to the periphery where nucleation takes place and solidification begins by the formation of equiaxed dendrites. Therefore, there can be considered as a start point of structure evolution for the cast product. Figure 3c represents the distribution of Copper within the solidifying billet. Enrichment in solidification region can be seen in this figure. More than anything, the distribution of composition is affected by the thermosolutal convections in the liquid and slurry regions and the permeability and the shrinkage flow in the semi-solid region.

The final distribution of the composition in solidified billet for the conditions given in case II is shown as relative macrosegregation profile across

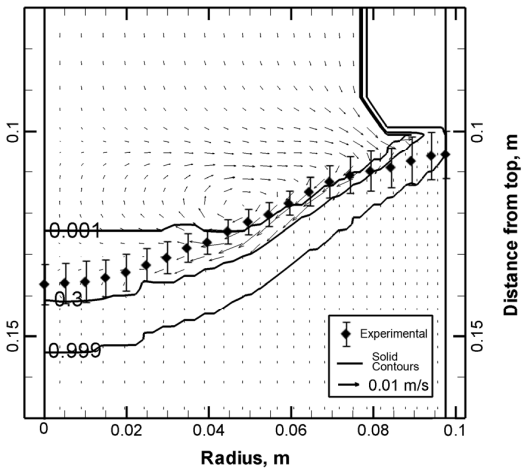

Fig. 2. Comparison of computed results for coherency line and experimental solidification front.

the radius of the billet in Figure 4. In this figure, the experimental measurements of composition with optical spectroscopy by Eskin et al [30] have been used as dark data points for comparison. Slight negative centre line segregation can be seen in the figure where the numerical result overestimates it. Towards the periphery, inverse segregation is dominant up to 7 cm from the center as the composition is increasing. With the same manner, numerical results show an increasing trend and give good estimation of the amount of segregation. At the outer radii, however, the effect of mold (primary) cooling appears with a sudden drop in composition and sever inverse segregation afterward. Numerical segregation pattern also reveals an oscillatory drop at the periphery which has been made smooth by interpolation. Generally the model is able to capture different regions and acceptably predict the inverse segregations. To precisely predict the surface segregation, the enriched liquid jet beneath the hottop should be properly considered, where the metal feeding, shrinkage flow and dendrite fragmentation combine to yield a supersaturated layer on the surface of the cast product as shown by a relatively high point of segregation in Figure 4. Thermosolutal convections in the liquid and slurry

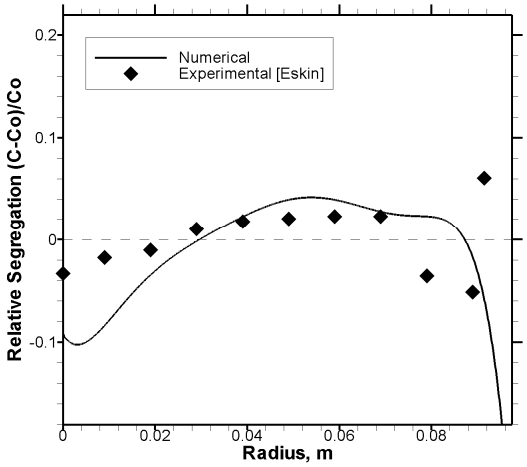

Fig. 4. Predicted macrosegregation profile within the cross section of the solidified billet.

regions and permeability and shrinkage flow in the semi-solid region show the dominant effect on the final macrosegregation pattern.

5. CONCLUSION

A numerical model was developed to study macrosegregation during DC casting of round billets of binary alloy. The problem was solved based on standard CV-FDM methods. However, a

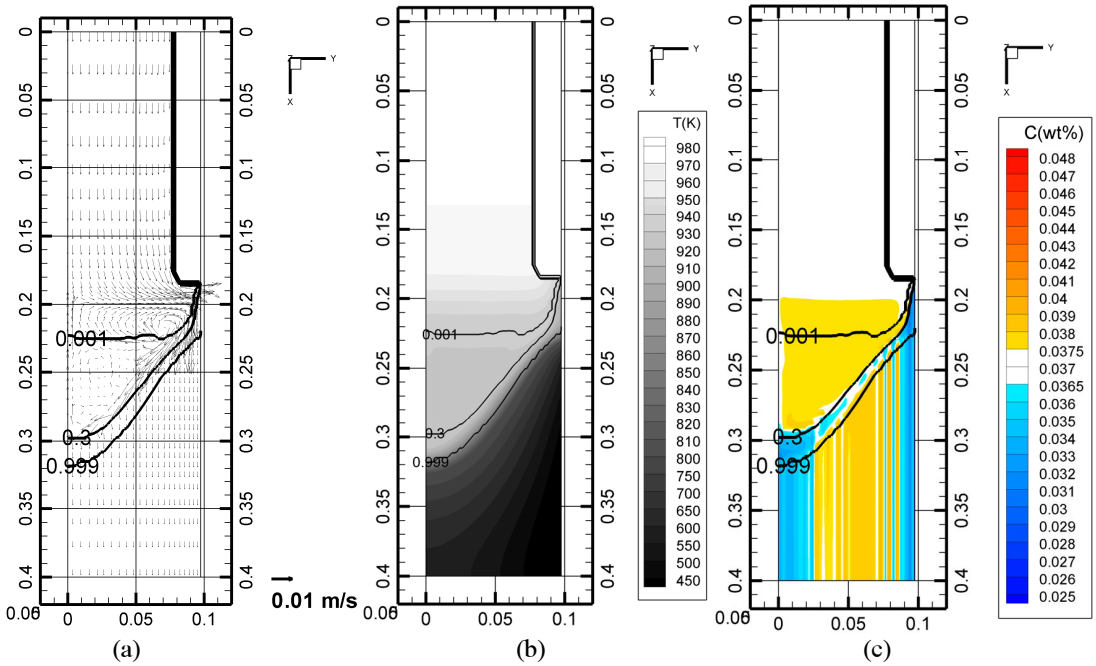

Fig. 3. Computed results for (a) velocity pattern (b) temperature field and (c) distribution of Copper in the alloy.

different solution methodology, called SIMTLE (Semi-Implicit Method for Thermodynamically-Linked Equations), was used to link energy and species equations with the thermodynamic phase diagram of the alloy. The methodology allows model to be flexible in using raw phase diagram data and to handle further physical complexities, but keeps the model simple, consistent and efficient in implementations.

The model was examined in two practical cases and the obtained results were compared with the experimental investigations on an industrial scale DC caster. The results (Figure 2 and Figure 4) reveal reasonable agreement with

NOMENCLATURE

Letters		**Greek Letters**	
a	coefficients of discretized equations	α	thermal diffusivity $= k/\rho c$
$\mathbf{B}$	body force vector	δ	diffusion length
C	composition*	ε	volume fraction
c	heat capacity*	ε_{SP}	packing solid volume fraction
D	coefficient of diffusion*	ϕ	general dependent variable
D^{ϕ}	diffusion-like source term	Γ	general diffusion coefficient
f	mass fraction	λ	under-relaxation factor
f'	correction for mass fraction	μ	viscosity*
F^{ϕ}	convection-like source term	ρ	density*
H	heat transfer coefficient	**Superscripts**	
h	enthalpy*	*	primary guess
h^{ref}	reference enthalpy*	C	solutal
K	permeability	eq	equilibrium
k	thermal conductivity*	ϕ	general dependent variable
$\mathbf{M}$	Interfacial drag force vector	new	updated value
n	grain density	T	thermal
p	pressure	**Subscripts**	
P	reduced pressure	α	α -phase
q	heat flux	β	β -phase
R	residual of the solution	C	casting
r	radial position	Cooling	cooling wall
S_V^{i}	interfacial area concentration	i	phase index
T	temperature	j	phase index
T^{eq}	Dynamic Implicit Equilibrium Temperature (DIET)	L	liquid
		e	eutectic
t	time	nb	neighbors of node P
x	distance in the coordinate	o	initial condition
u	velocity component in axial position	P	node P
$\mathbf{v}$	velocity vector*	ref	reference
v	velocity component in radial position	S	solid
z	axial position		

* Variables without a phase index refer to the mixture.

the experiments. The results were also discussed in the form of flow patterns and distribution of the alloying element. Thermosolutal convections in the liquid and slurry regions and permeability and shrinkage flow in the semi-solid region show the dominant effect on the final macrosegregation pattern. It is concluded that a proper and reliable macrosegregation model needs two key features: a precise flow description in the two-phase regions and a capable efficient numerical scheme to solve it.

ACKNOWLEDGMENT

The authors would like to gratefully acknowledge the supply of Department of Materials Science Engineering at Delft University of Technology (TUDelft) for providing the experimental data which were crucial to complete this work.

REFERENCES

1. Nadella, R., Eskin, D. G., Du, Q., Katgerman, L., Macrosegregation in Direct-Chill Casting of Aluminium Alloys, Progress in Materials Science, 53 (2008) 421-480.
2. Flemings, M. C., Our Understanding of Macrosegregation: Past and Present, ISIJ International, 40 (2000) 833-841.
3. Beckermann, C., Modelling of Macrosegregation: Applications and Future Needs, International Materials Reviews, 47 (2002) 243-261.
4. Devadas, C., Grandfield, J. F., "Experiences with Modelling Dc Casting of Aluminum," in Proceedings of the 120th TMS Annual Meeting Light Metals, TMS Annual Meeting: TMS (The Minerals, Metals & Materials Society), 1990, pp. 883-892.
5. Du, Q., Eskin, D. G., Katgerman, L., Modeling Macrosegregation During Direct-Chill Casting of Multicomponent Aluminum Alloys, Metall. Mater. Trans. A, 38A (2007) 180-188.
6. Eskin, D. G., Du, Q., Katgerman, L., Scale Rules for Macrosegregation During Direct-Chill Casting of Aluminum Alloys, Metall. Mater. Trans. A, 39A (2008) 1206-1212.
7. Reddy, A. V., "Two-Phase Simulation of the Direct Chill Continuous Casting of Al-Cu Round Ingots," in Mechanical Engineering in the Graduate College Iowa City: The University of Iowa, 1995, p. 171.
8. Mo, A., Mathematical Modelling of Surface Segregation in Aluminum Dc Casting Caused by Exudation, Int. J. Heat Mass Transfer, 36 (1993) 4335-4340.
9. Nadella, R., Eskin, D. G., Katgerman, L., Role of Grain Refining in Macrosegregation Upon Direct Chill Casting of Aa 2024 Round Billet, Materials Science Forum, 519-521 (2006) 1841-1846.
10. Rerko, R. S., Groh, H. C. D., Beckermann, C., Effect of Melt Convection and Solid Transport on Macrosegregation and Grain Structure in Equiaxed Al-Cu Alloys, Materials Science and Engineering A, A347 (2003) 186-197.
11. Krane, M. J. M., Vusanovic, I., Macrosegregation in Horizontal Direct Chill Casting of Aluminium Slabs, Mater. Sci. Technol., 25 (2009) 102-107.
12. Venneker, B. C. H., Katgerman, L., Modelling Issues in Macrosegregation Predictions in Direct Chill Castings, Journal of Light Metals, 2 (2002) 149-159.
13. Vreeman, C. J., Incropera, F. P., Numerical Discretization of Species Equation Source Terms in Binary Mixture Models of Solidification and Their Impact on Macrosegregation in Semicontinuous, Direct Chill Casting Systems, Numer. Heat Transfer, Part B, 36 (1999) 1-14.
14. Vreeman, C. J., Schloz, J. D., Krane, M. J. M., Direct Chill Casting of Aluminum Alloys: Modeling and Experiments on Industrial Scale Ingots, Journal of Heat Transfer, Transactions of the ASME, 124 (2002) 947-953.
15. Zaloznik, M., Sarler, B., "New Insights into Flow Structure in the Dc Casting of Aluminum Alloys," in Light Metals 2005, TMS Annual Meeting, H. Kvande, Ed. San Francisco, CA, USA: TMS (The Minerals, Metals & Materials Society), 2005, pp. 1031-1036.
16. Zaloznik, M., Sarler, B., Melt Flow and Macrosegregation in Dc Casting of Aluminum Alloys, Materials Science Forum, 508 (2006) 515-522.
17. Vreeman, C. J., Incropera, F. P., The Effect of

Free-Floating Dendrites and Convection on Macrosegregation in Direct Chill Cast Aluminum Alloys Part Ii: Predictions for Al-Cu and Al-Mg Alloys, Int. J. Heat Mass Transfer, 43 (2000) 687-704.

18. Vreeman, C. J., Krane, M. J. M., Incropera, F. P., The Effect of Free-Floating Dendrites and Convection on Macrosegregation in Direct Chill Cast Aluminum Alloys Part I: Model Development, Int. J. Heat Mass Transfer, 43 (2000) 677-686.
19. Bennon, W. D., Incropera, F. P., A Continuum Model for Momentum, Heat and Species Transport in Binary Solid-Liquid Phase Change Systems - I. Model Formulation, Int. J. Heat Mass Transfer, 30 (1987) 2161-2170.
20. Ni, J., Beckermann, C., A Volume-Averaged Two-Phase Model for Transport Phenomena During Solidification, Metall. Mater. Trans. B, 22b (1991) 349-361.
21. Ni, J., Incropera, F. P., Extension of the Continuum Model for Transport Phenomena Occurring During Metal Alloy Solidification - I. The Conservation Equations, Int. J. Heat Mass Transfer, 38 (1995) 1271-1284.
22. Prescott, P. J., Incropera, F. P., Bennon, W. D., Modeling of Dendritic Solidification Systems: Reassessment of the Continuum Momentum Equation, Int. J. Heat Mass Transfer, 34 (1991) 2351-2359.
23. Poirier, D. R., Ganesan, S., Permeabilities for Flow of Interdendritic Liquid in Equiaxial Structures, Materials Science & Engineering A: Structural Materials: Properties, Microstructure and Processing, 157 (1992) 113-123.
24. Ni, J., Incropera, F. P., Extension of the Continuum Model for Transport Phelnomena Occurring During Metal Alloy Solidification - Ii. Microscopic Considerations, Int. J. Heat Mass Transfer, 38 (1995) 1285-l296.
25. Eskin, D. G., Zuidema, J., Savran, V. I., Katgerman, L., Structure Formation and Macrosegregation under Different Process Conditions During Dc Casting, Materials Science and Engineering A, 384 (2004) 232-244.
26. Versteeg, H. K., Malalasekera, W., An Introduction to Computational Fluid Dynamics, Finite Volume Method, Longman Group Ltd., London, 1995.
27. Patankar, S. V., Numerical Heat Transfer and Fluid Flow, Hemisphere Publishing Corporation, USA, 1980.
28. Jafari, A., Seyedein, S. H., Aboutalebi, M. R., Semi-Implicit Method for Thermodynamically Linked Equations in Phase Change Problems (Simtle), Part I - Basic Structure, Appl. Math. Modell., Submitted (2009)
29. Eskin, D. G., Jafari, A., Katgerman, L., Contribution of Forced Centreline Convection During Direct-Chill Casting of Round Billets to Macrosegregation and Structure of a Binary Al-Cu Aluminium Alloy, Mater. Sci. Technol., In Press (2009)
30. Eskin, D. G., Nadella, R., Katgerman, L., Effect of Different Grain Structures on Centerline Macrosegregation During Direct-Chill Casting, Acta Mater., 56 (2008) 1358-1365.